Chemical pressure effect on the optical conductivity of the nodal-line semimetals ZrSiY (Y = S, Se, Te) and ZrGeY (Y = S, Te)

J. Ebad-Allah,[1,2] J. Fernández Afonso,[3] M. Krottenmüller,[1] J. Hu,[4] Y. L. Zhu,[5,6] Z. Q. Mao,[5,6] J. Kuneš,[3,7,*] and C. A. Kuntscher[1,†]

[1]*Experimentalphysik II, Augsburg University, 86159 Augsburg, Germany*
[2]*Department of Physics, Tanta University, 31527 Tanta, Egypt*
[3]*Institute of Solid State Physics, TU Wien, 1020 Vienna, Austria*
[4]*Department of Physics, University of Arkansas, Fayetteville, Arkansas 72701, USA*
[5]*Department of Physics, Pennsylvania State University, University Park, Pennsylvania 16803, USA*
[6]*Department of Physics and Engineering Physics, Tulane University, New Orleans, Louisiana 70118, USA*
[7]*Institute of Physics, The Czech Academy of Sciences, 18221 Praha, Czech Republic*

(Received 10 December 2018; published 29 March 2019)

ZrSiS is a nodal-line semimetal, whose electronic band structure contains a diamond-shaped line of Dirac nodes. We carried out a comparative study on the optical conductivity of ZrSiS and the related compounds ZrSiSe, ZrSiTe, ZrGeS, and ZrGeTe by reflectivity measurements over a broad frequency range combined with density functional theory calculations. The optical conductivity exhibits a distinct U shape, ending at a sharp peak at around 10 000 cm^{-1} for all studied compounds except for ZrSiTe. The U shape of the optical conductivity is due to transitions between the linearly dispersing bands crossing each other along the nodal line. The sharp high-energy peak is related to transitions between almost parallel bands, and its energy position depends on the interlayer bonding correlated with the c/a ratio, which can be tuned by either chemical or external pressure. For ZrSiTe, another pair of crossing bands appears in the vicinity of the Fermi level, corrugating the nodal-line electronic structure and leading to the observed difference in optical conductivity. The findings suggest that the Dirac physics in ZrXY compounds with X = Si, Ge and Y = S, Se, Te is closely connected to the interlayer bonding.

DOI: 10.1103/PhysRevB.99.125154

I. INTRODUCTION

The quest for novel topological materials with exceptional properties has led in recent years to an enormous research activity on two-dimensional (2D) and three-dimensional (3D) Dirac semimetals hosting massless Dirac fermions. In Dirac semimetals, linearly dispersing bands cross at isolated points at the Fermi energy E_F, resulting in a dispersion locally resembling that of massless fermions. The most popular example for a 2D Dirac semimetal is graphene exhibiting highly interesting properties, such as outstanding mechanical stability [1], ultrahigh electron mobility [2], and superior thermal conductivity [3]. In contrast to Dirac semimetals with discrete Dirac points or nodes, in nodal-line semimetals, the linearly dispersing bands cross along a line in the Brillouin zone. Corrugation of the nodal lines in the energy direction then gives rise to rod-shaped Fermi surfaces, which are sensitive to small changes in external parameters.

ZrSiS is a nodal-line semimetal with a diamond-rod-shaped Fermi surface resulting from an almost ideal nodal-line band structure [4]. It was suggested that its band structure contains additional Dirac-like band crossings located several hundred meV above and below E_F, which are protected by nonsymmorphic symmetry [5–7]. ZrSiS is exceptional among the Dirac materials since the linearly dispersing bands at E_F extend over a rather large energy range of up to 2 eV, although spin-orbit coupling (SOC) introduces a small gap (∼0.02 eV) to the Dirac nodes. It shows exceptional properties, such as unusual magnetoresistance characteristics [8,9], high mobility of charge carriers [9,10], and correlation effects [11], which renders ZrSiS a highly interesting material.

ZrSiS belongs to the family of compounds ZrXY, where X can be a carbon group element (X = Si, Ge, Sn) and Y is a chalcogen element (Y = S, Se, Te) [12]. In this compound family, the 2D-to-3D structural dimensionality evolution induced by isoelectronic substitution, which is generally called chemical pressure, was suggested to be realized and to be monitored *via* the ratio of lattice parameters c/a [12,13]. This renders ZrXY a model system to probe the effect of structural dimensionality change in nodal-line semimetals.

Earlier optical studies on ZrSiS found a rather flat optical conductivity in the energy range of 30–300 meV, which was claimed to be due to 2D Dirac bands near E_F [14]. This interpretation was, however, questioned recently by theoretical calculations [15]. The high-energy optical conductivity exhibits a distinct U shape ending at a sharp kink/peak around 10 000 cm^{-1}, which was not addressed previously [14].

We present a combined experiment + theory study of several members of the ZrXY family, which addresses these features and relate them to the nodal-line electronic structure of

*kunes@ifp.tuwien.ac.at
†christine.kuntscher@physik.uni-augsburg.de

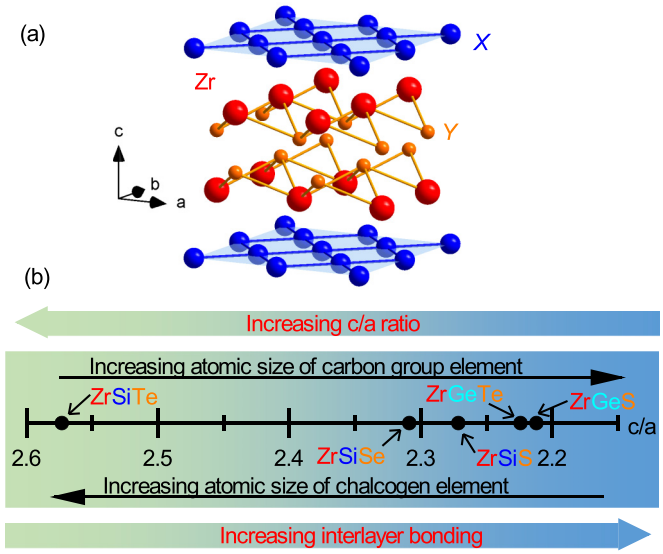

FIG. 1. (a) Crystal structure of the ZrXY compounds with square nets parallel to the *ab* plane. (b) Scheme illustrating the chemical pressure effect in ZrSiS, ZrSiSe, ZrSiTe, ZrGeS, and ZrGeTe.

the materials. In particular, we find that ZrSiS, ZrSiSe, ZrGeS, and ZrGeTe have very close to ideal nodal-line band structures with varying degrees of corrugation of the nodal line, whereas in ZrSiTe another pair of crossing bands appears in the vicinity of the Fermi level, destroying the nodal-line structure and pushing it away from E_F in parts of the Brillouin zone.

The compounds ZrXY crystallize in a PbFCl-type structure in the tetragonal $P4/nmm$ space group with nonsymmorphic symmetry [see Fig. 1(a)] [12]. The layered crystal structure contains square nets of X atoms parallel to the *ab* plane where each X square net is sandwiched between two Zr square nets. Each X atom has bonding to four Zr atoms in tetrahedral coordination. The chalcogen atoms Y also form square nets on the *ab* plane. Hence, the crystal structure of ZrXY consists of slabs with five square nets with a stacking sequence [Y-Zr-X-Zr-Y], terminated by Y square nets on both sides [9]. The bonding between two adjacent slabs was suggested to be of van der Waals type and hence weak. Therefore, these crystals generally tend to cleave along the plane between two chalcogen layers.

It was proposed that the structural dimensionality of the ZrXY materials can be tuned by chemical pressure, i.e., isoelectronic substitution, and monitored *via* the ratio of lattice parameters c/a, where c is the distance between two adjacent Si square nets and a is the in-plane lattice parameter of the tetragonal crystal structure [12,13]. The c/a ratio may serve as a measure for the interlayer bonding strength in the system. As illustrated in Fig. 1(b), the chemical pressure effect in the studied ZrXY compounds can be realized either by the isoelectronic substitution of the carbon group element X or by the chalcogen element Y. With increasing the atomic size of the chalcogen element Y, the slab thickness along the c axis increases, and hence the c/a ratio increases, causing a decrease in the interlayer bonding. Accordingly, the chemical pressure in ZrSiTe is reduced as compared to ZrSiS, and therefore ZrSiTe was described as a layered material without significant interlayer bonding [12]. In contrast, with increasing atomic size of the carbon group element X, the c/a ratio decreases and thus tunes the interlayer bonding in the opposite way. For example, in ZrSiS, a smaller interlayer bonding is expected as compared to ZrGeS [see Fig. 1(b)]. In the case of the X substitution, the chemical pressure effect is, however, less direct as described in Ref. [12]: The increasing atomic size of X leads to longer X-X bonds within the X square nets, which affects the in-plane Y-Y spacing as well. The cell parameter c is decreased, whereas the unit cell expands along the a direction. The net effect is an enhancement of the interlayer bonding in adjacent [Y-Zr-X-Zr-Y] slabs.

Among all studied materials, ZrSiTe has the highest c/a ratio with a value close to 2.6, and therefore supposedly has a smaller interlayer bonding. This is confirmed by de Haas–van Alphen quantum oscillation measurements, which show that the Fermi surface has a 2D character in ZrSiTe, in contrast to ZrSiS and ZrSiSe (c/a ratio close to 2.3) with a 3D-like Fermi surface [16]. This also explains why ZrSiTe single crystals can be easily exfoliated mechanically.

II. SAMPLE PREPARATION, EXPERIMENTAL AND COMPUTATIONAL DETAILS

Single-crystals ZrSiY (Y = S, Se, Te) and ZrGeY (Y = S, Te) were grown by a chemical-vapor transport method [10,17]. The samples were characterized by x-ray diffraction and energy-dispersive x-ray spectroscopy in order to ensure phase purity and crystal quality.

The reflectivity measurements were carried out in the frequency range ($\approx$100–24 000 cm^{-1}) with an infrared microscope (Bruker Hyperion), equipped with a 15$\times$ Cassegrain objective, coupled to a Bruker Vertex v80 Fourier-transform infrared spectrometer. Reflectivity measurements on ZrSiSe, ZrSiTe, and ZrGeTe were performed on freshly cleaved (001) surfaces. Since ZrSiS and ZrGeS crystals cannot be easily cleaved, the as-grown, shiny (001) surfaces were carefully cleaned with isopropanol before the reflectivity measurements. The reproducibility of the results was checked on several crystals for each compound. To obtain the absolute reflectivity spectra, the intensity reflected from an Al mirror served as the reference. The reflectivity measurements were carried out at room temperature since the dependence of the optical response on temperature is relatively weak especially regarding the interband transitions as was shown for ZrSiS [14].

The frequency-dependent dielectric function $\epsilon(\omega)$ and optical conductivity $\sigma(\omega)$ of the materials were obtained via Kramers-Kronig analysis of the reflectivity spectra. To this end, the reflectivity data were extrapolated to low frequencies based on the Drude-Lorentz fitting, whereas x-ray atomic scattering functions [18] were used for calculating the higher-frequency extrapolations. A power-law $1/\omega^n$ with n up to 3 was used for interpolating the reflectivity spectra between the measured and the calculated data. The contributions to the optical conductivity spectra σ_1 were obtained by simultaneous Drude-Lorentz fitting of the reflectivity and optical conductivity.

Pressure-dependent reflectance measurements up to 3.5 GPa at room temperature were carried out with an infrared microscope (Bruker Hyperion) coupled to a Bruker Vertex v80

Fourier-transform infrared spectrometer in the frequency range of 600–23 000 cm^{-1}. All the pressure-dependent reflectivity spectra refer to the absolute reflectivity at the sample-diamond interface, denoted as R_{sd}. The reflectivity spectrum $R_{sd}(\omega)$ was calculated according to $R_{sd}(\omega) = R_{dia} \times I_s(\omega)/I_{ref}(\omega)$, where I_s is the intensity of the radiation reflected from the sample-diamond interface, I_{ref} is the intensity reflected from the inner diamond-air interface of the empty diamond-anvil cell, and $R_{dia} = 0.167$, which is assumed to be pressure independent [19].

The pressure-dependent reflectivity spectra are affected in the frequency range between 1800 and 2670 cm^{-1} by multiphonon absorptions in the diamond anvils, which are not completely corrected by the normalization procedure. Therefore, this part of the spectrum was interpolated based on the Drude-Lorentz fitting. The measured reflectivity data were extrapolated to low frequencies based on the Drude-Lorentz fit for further analysis. For the high-frequency extrapolation the simulated free-standing reflectivity spectrum (see above) was used, taking into account the sample-diamond interface. The real part of the optical conductivity σ_1 was obtained via Kramers-Kronig transformation of the reflectivity spectrum [20].

Density functional theory (DFT) calculations have been performed using the WIEN2K [21] code. The calculations were carried out with the generalized gradient approximation as the exchange-correlation functional, 1000 k points in the self-consistent calculation and 200 000 k points to evaluate the optical conductivity.

In order to gain insight into the origin of the studied band structures, we have constructed a tight-binding model in the basis of Zr-d, Si-s, p, and Y-p Wannier functions. To this end we have used the WANNIER90 [22] and WIEN2WANNIER [23] packages.

III. RESULTS

The real part of the optical conductivity $\sigma_1(\omega)$ of ZrSiS (see Fig. 2, and Fig. S2(a) in the Supplemental Material [28]) contains two Drude contributions, which is consistent with recent reports of the coexistence of electron-type and hole-type charge carriers where electron-hole compensation was suggested to cause an extremely large magnetoresistance [8,24]. Besides the Drude contributions, the low-energy optical conductivity shows a plateaulike behavior in the range of ~240–2400 cm^{-1}, which was claimed to be due to 2D Dirac bands near E_F [14]. In analogy to graphene, in a 2D system with an ideal linear dispersion of Dirac bands, one would expect a constant optical conductivity [25–27]. The interpretation of the flat conductivity in ZrSiS in terms of 2D Dirac bands was, however, questioned recently by theoretical calculations [15]. The drop in the optical conductivity for higher frequencies and the subsequent rise result in a broad dip centered at 6700 cm^{-1}, i.e., a U-shaped optical conductivity [see Figs. 2 and 3(a)]. The high-energy optical conductivity of ZrSiS is rather flat, overlayed with three well-resolved absorption features, which have not been considered previously. Among them, the sharp peak at 11 650 cm^{-1} [labeled L4 in Fig. 3(b)] is the most pronounced. A similar profile of the optical conductivity spectrum—namely, a distinct U shape ending at a sharp peak—is found for the materials ZrSiSe, ZrGeS, and ZrGeTe (see Figs. 2 and 3). In particular, the high-energy L4 peak is present in all three compounds with slight variation in its energy position depending on the carbon group element and the chalcogen element (chemical pressure).

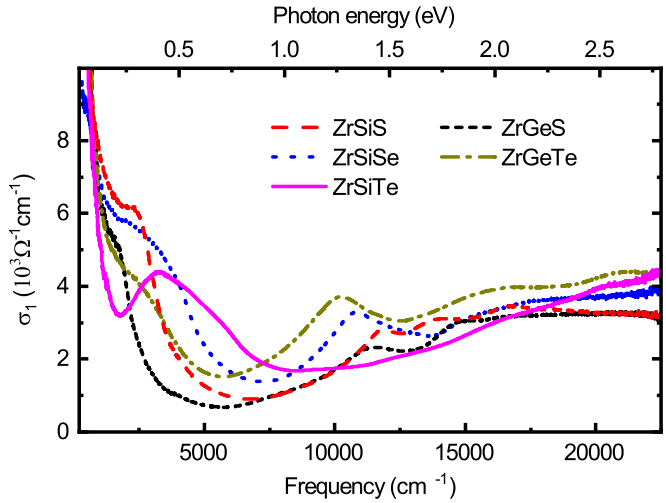

FIG. 2. Experimental optical conductivity spectra for all measured ZrXY compounds as obtained from ambient-condition reflectivity spectra.

In comparison to the other studied ZrXY materials, the optical conductivity profile of ZrSiTe is distinctly different [see Figs. 2 and 3(d)]. Besides the Drude-like characteristics, the low-energy range is dominated by a pronounced absorption band centered at ≈3300 cm^{-1} with a shoulder on its high-frequency side (see Fig. S2(c) in the Supplemental Material [28]). Above 9000 cm^{-1}, the optical conductivity monotonically increases with increasing frequency without any well-resolvable feature. Most importantly, the sharp peak at around 10 000 cm^{-1} is no longer present in ZrSiTe.

A. Theoretical optical spectra

In order to understand the measured optical conductivities, we have performed density functional calculations with the WIEN2K [21] code for obtaining the electronic band structure and optical spectra. Here, we focus on the high-energy features in the optical spectra > 3000 cm^{-1}, and thus we did not consider the Drude intraband contributions. The spin-orbit coupling plays no role in the optical conductivity in this frequency range. Starting from the scalar-relativistic (no spin-orbit coupling) band structure, the spin-orbit coupling opens or enhances a small gap between the crossing bands forming the nodal line in the vicinity of the Fermi level. It thus affects the dc electrical transport and low-energy optical conductivity, however, being restricted to a low-dimensional subspace (vicinity of the nodal line) of the Brillouin zone, the spin-orbit splitting was found to have no discernible effect on the optical conductivity in the frequency range of > 3000 cm^{-1}.

The comparison in Fig. 3 reveals a good quantitative agreement between experiment and theory for all studied compounds. With ZrSiTe being a clear outlier, all the remaining compounds exhibit a U-shaped optical conductivity between 3000 and 10 000 cm^{-1}, bounded on the low-energy

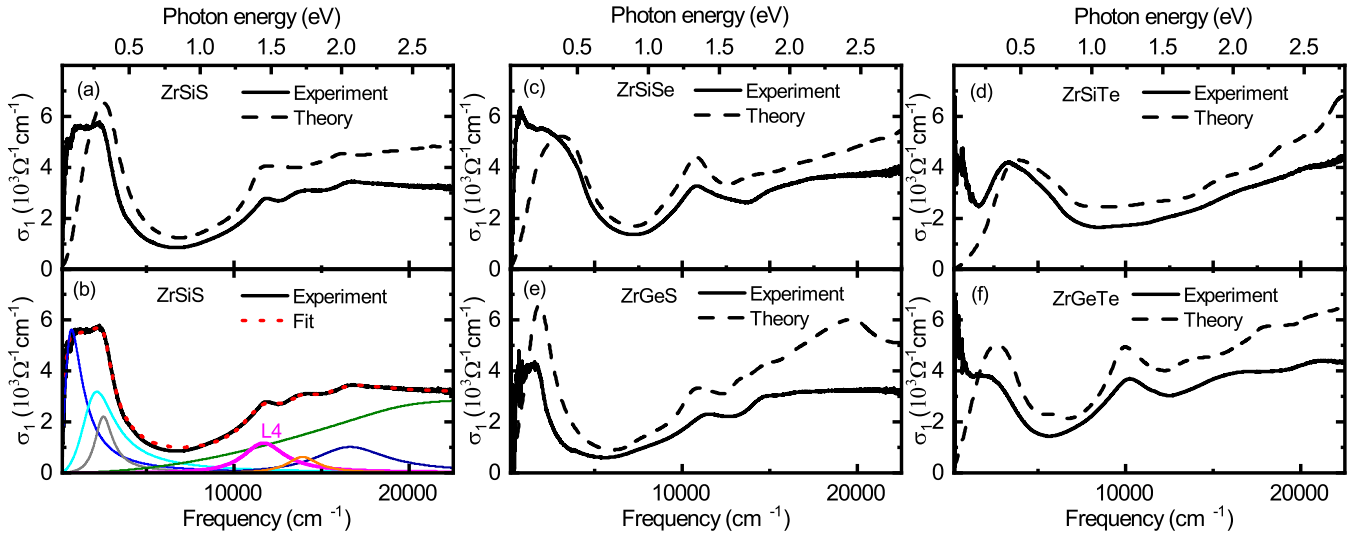

FIG. 3. (a) and (c)–(f) Comparison of the experimental and theoretical optical conductivities without intraband contributions for ZrSiS, ZrSiSe, ZrSiTe, ZrGeS, and ZrGeTe, respectively. (b) Contributions to the experimental optical conductivity of ZrSiS as obtained from the fitting are shown, in particular, the sharp peak labeled L4, which is due to transitions between almost parallel bands.

side by a flat region and on the high-energy side by a sharp peak (see Fig. 3). In order to understand the origin of these features, we show the calculated band structure together with a decomposition of the optical conductivity and JDOS into contributions of different band combinations in Fig. 4. We point out that this decomposition is merely an analytic tool and does not have a deeper physical meaning.

First, we discuss the spectrum of ZrSiS. The dropping side of the U-shaped region of the optical conductivity spectrum (<6000 cm^{-1}) is dominated by the transitions between the

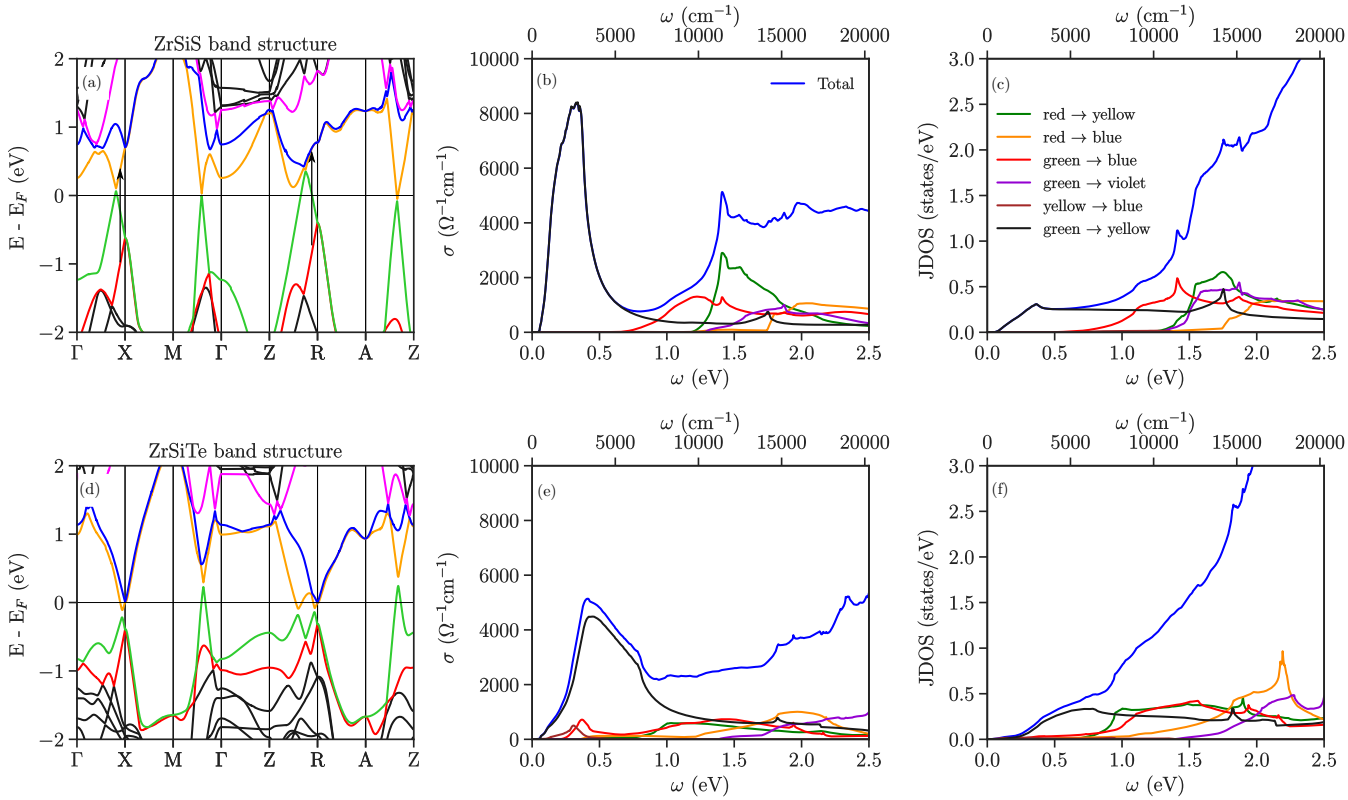

FIG. 4. Calculated band structures of (a) ZrSiS and (d) ZrSiTe with SOC, panels (b) and (e) and (c) and (f) show contributions of different band combinations to the optical conductivity σ and the joint density of states (JDOS), respectively. The black arrows in panel (a) highlight the transitions between almost parallel red and yellow bands in the vicinity of the X and R points, which give rise to the L4 peak in the optical conductivity.

linear crossing bands close to E_F, marked green and yellow in Fig. 4(a). The rising side of the U-shaped region is due to other band combinations. Analyzing the band and k-point contribution to the optical conductivity, the sharp L4 kink marking the upper bound of the U-shaped region can be assigned to transitions between the almost parallel red and yellow bands in the vicinity of the X and R points as marked in Fig. 4(a). This interpretation was first pointed out by Habe and Koshino [15]. Therefore, the position of the kink in all the studied materials, except for ZrSiTe, follows the red/yellow band splitting at the X and R points.

The comparison of the optical conductivity in Fig. 4(b) with the JDOS in Fig. 4(c) reveals an approximate $1/\omega$ relationship between the two quantities, which corresponds to constant momentum dipole matrix elements [25,27] (see the Supplemental Material Fig. S4 [28]). The JDOS originating from the lowest bands exhibits a broad constant region following the initial onset [black line in Fig. 4(c)]. The constant region of JDOS reflects the linear relative dispersion of the valence (green) and conduction (yellow) bands. This dispersion is effectively one dimensional (1D): linear in the direction perpendicular to the nodal line, whereas almost constant along the nodal line as well as in the z direction due to the quasi-2D electronic structure. Such a 1D linear dispersion gives rise to a constant JDOS. The onset region reflects the deviation from this idealization due to corrugation of the nodal line and gap opening in the bulk of the Brillouin zone. We observe numerically that in all the studied materials the low-frequency limit of the U-shaped region correlates with the boundary of the constant JDOS. Our analysis thus does not confirm the interpretation of Ref. [14], which ascribed the spectra between 250 and 2500 cm^{-1} to the linear bands and estimated the deviations from the nodal-line shape due to gap opening or shift away from the Fermi level to 30 meV. Our numerical results suggest the deviations from the perfect nodal-line structure to be an order of magnitude bigger, largely due to corrugation of the nodal line (shift away from the Fermi level).

To summarize, the U shape of the optical conductivity reflects the proximity to an idealized band structure with two linearly crossing (touching) bands along a surface in the Brillouin zone, forming an effective nodal plane. The low-frequency boundary correlates with the deviations from this idealized picture due to gapping of the bands or shifting the band crossings away from the Fermi level [29].

The only exception is ZrSiTe. In this compound, another pair of bands approaches the Fermi level in the vicinity of the X-R line [see Fig. 4(d)]. Besides distorting the nodal-line structure in this part of the reciprocal space, the Fermi level is pushed away from the nodal line in the rest of the Brillouin zone. As a result, the optical conductivity spectrum depicted in Fig. 4(e) changes its shape substantially.

B. Band structure of ZrXY

In order to understand the band structure of the ZrXY compounds, we have constructed a tight-binding model on the basis of Wannier orbitals with Zr d, Si s, p, and S (Te) p characters. In this way, the valence and low-energy conduction bands are represented exactly, whereas the higher-lying conduction bands of Si p and Zr d characters are disentangled from the rest of the band structure. Next, we have calculated a series of band structures including an increasing number of hopping processes.

In the first (upper) row of Fig. 5, only the nearest-neighbor Si-Si (in-plane) hopping is taken into account. Even this simple model captures the gross features of the ZrXY band structure, i.e., flat empty Zr-d and occupied S(Te)-p bands overlaid with broad 2D Si-sp bands. Whereas the Si-p_z bands will be removed from the Fermi level due to the interlayer hybridization, the crossings of Si-p_xp_ys bands are the precursors of the nodal line.

In the second row [Figs. 5(c) and 5(d)], the nearest-neighbor Si-Si, Si-Zr, and Zr-S(Te) hoppings are included. We note that strong Zr-Si-p_z hybridization removes the p_z bands from the vicinity of the Fermi level, eventually forming a flat valence band between -1 and -2 eV as well as contributing to the conduction band above 5 eV. The Zr-Si-p_xp_ys hybridization is stronger. A typical shape arising from hybridization between broad and narrow bands can be observed. The band crossing of Si-p_xp_ys bands from the upper row of Fig. 5 are now doubled, forming Si-Zr bonding and antibonding counterparts below and above the Zr-d manifold. The band structure obtained with unlimited hopping, depicted in Figs. 5(e) and 5(f), exhibits only quantitative deviations from the one in the second row.

To summarize, the gross features of the electronic structure of ZrXY can be understood as an overlap of broad sp bands of a single X layer with much narrower Zr-d (empty) and Y-p bands (full). The precursor of the nodal line can be found in the crossing of backfolded X-sp_xp_y bands. Hybridization with the Zr layer removes the X-p_z bands from the vicinity of E_F, whereas the X sp_xp_y-Zrd hybrid forms the nodal line.

IV. DISCUSSION

Angle-resolved photoemission experiments on ZrSiS combined with electronic band-structure calculations found a diamond-shaped 3D-like Fermi surface due to a line of Dirac nodes [5,6]. Furthermore, it was suggested that the electronic band structure of ZrSiS contains additional Dirac-like band crossings located several hundred meV above and below E_F at the X and R points of the Brillouin zone. These band crossings are protected by nonsymmorphic symmetry against gapping due to the spin-orbit coupling. A comparative study on ZrSiS, ZrSiSe, and ZrSiTe proposed that the energy positions of these band crossings depend on the c/a ratio [6,7,30], which may serve as a measure for the interlayer bonding [12]. Whereas in ZrSiS the band crossings are located at 0.5–0.7 eV above and below E_F, for layered ZrSiTe without significant interlayer bonding, they are located close to E_F [7], i.e., with increasing c/a ratio the band crossings shift towards E_F. It was also suggested that the electronic structure is very similar for the compounds ZrXY (X = Si, Ge; Y = S, Se, Te) *including* ZrSiTe with only a fine-tuning due to the chemical pressure effect [7,16].

According to our findings, the qualitative similarities in the electronic structure and optical conductivity only hold for compounds ZrXY with a similar chemical pressure (for the c/a ratios close to 2.2 to 2.3). In stark contrast, ZrSiTe with a significantly larger c/a ratio [see Fig. 1(b)] and hence

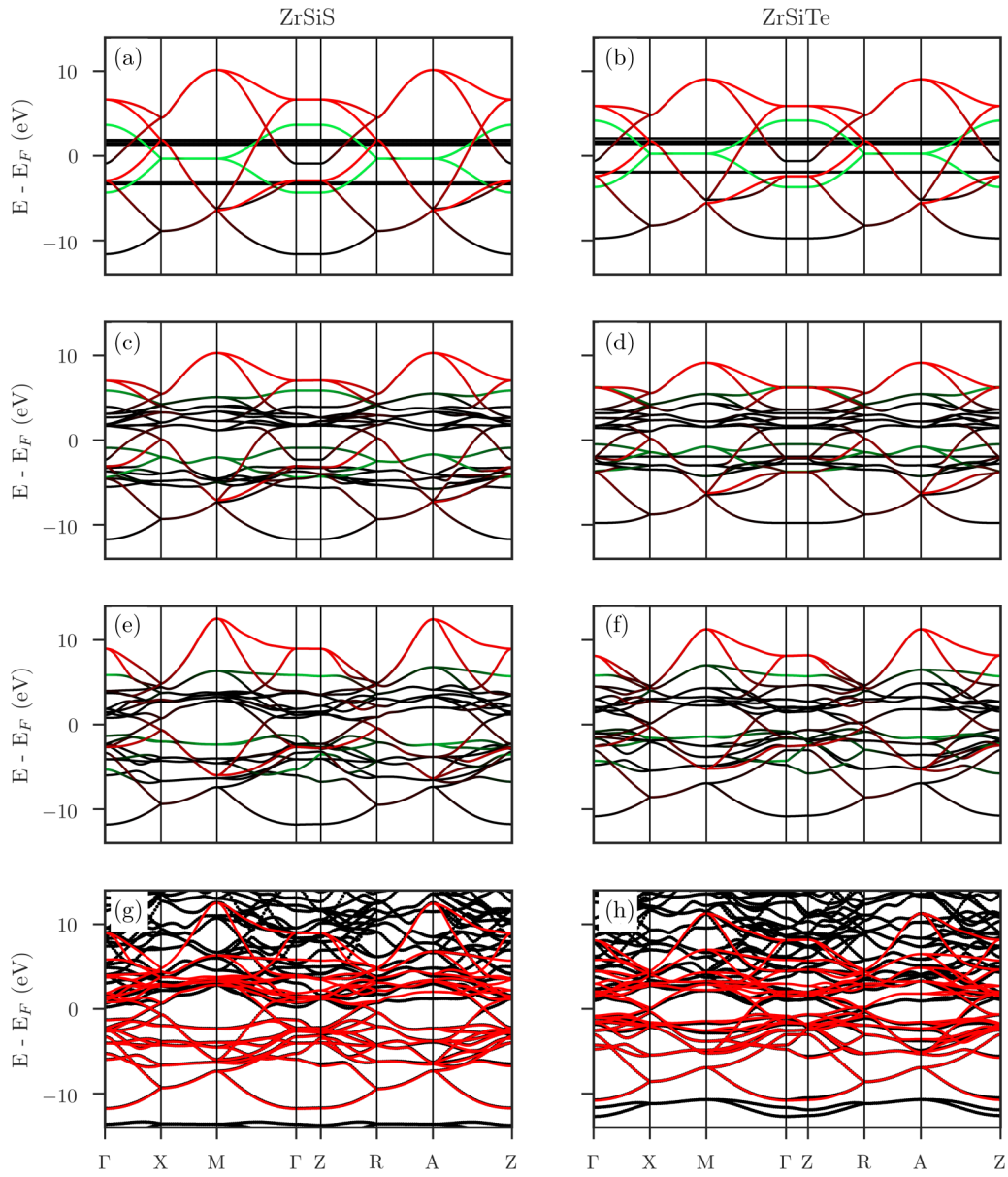

FIG. 5. Wannier band structures of ZrSiS (left) and ZrSiTe (right). The red and green colors in panels (a)–(f) reflect the Si $pxpy$ and Si pz weights, respectively. Panels (a)–(f) show the band structures obtained for hopping constrained to: nearest neighbors on the Si plane (a) and (b), nearest-neighbors Si-Si, Si-Zr, and Zr-S/Te (c) and (d), and no constraints (e) and (f). Panels (g) and (h) show the same Wannier band structure (red) as panels (e) and (f) compared to the full DFT band structures (black).

smaller interlayer bonding, behaves distinctly different. In particular, the compounds ZrSiS, ZrSiSe, ZrGeS, and ZrGeTe all show the sharp L4 peak in the optical conductivity, where its energy position depends on the specific compound and presumably on the c/a ratio. For a quantitative analysis, we fitted the experimental optical conductivity spectra with the Drude-Lorentz model and obtained the energy position of the L4 peak for all studied compounds (see Fig. S2 in the Supplemental Material [28]). In Fig. 6(a), the energy of the L4 peak is plotted as a function of the c/a ratio for ZrSiS, ZrSiSe, ZrGeS, and ZrGeTe, together with the positions from our theoretical results. We find that with the increasing c/a ratio (decreasing chemical pressure) the sharp L4 peak shifts to lower energies. This holds for ZrSiSe as compared to ZrSiS, and for ZrGeTe as compared to ZrGeS. However, when comparing ZrSiS with ZrGeS, it seems that a simple chemical pressure effect is not strictly given for the replacement of the carbon group element. Apparently, the simple correlation between chemical pressure and peak position does not strictly hold for substitutions in the X square nets. This might be due to the indirect character of the chemical pressure effect induced by the X substitution as already described in the Introduction.

The L4 peak in the optical conductivity stems from transitions between almost parallel bands in the vicinity of the X and the R points of the Brillouin zone as described above. At the same k points, the ungapped Dirac-like band crossings are located [6,7]. Therefore, the L4 peak might be related to the band crossings at the X and R points, respectively. In order to check this, we compare in Fig. 6(a) the energy difference ΔE between the ungapped band crossings above and below

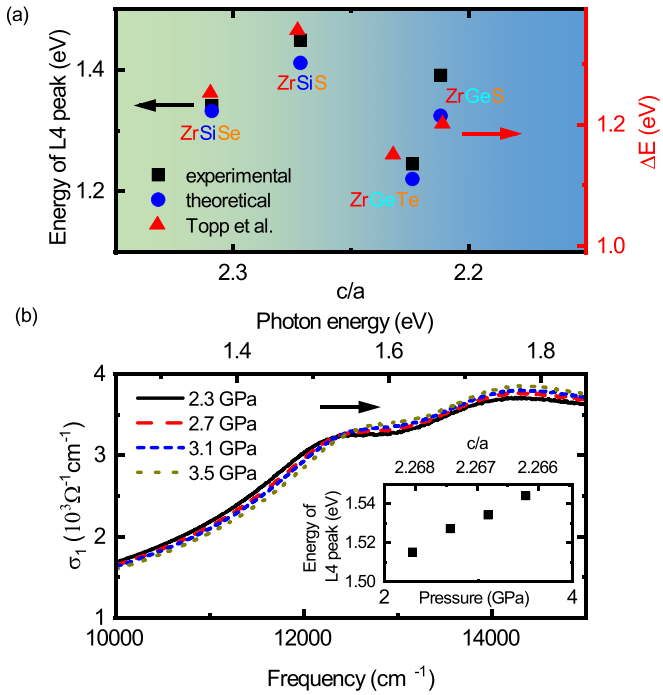

FIG. 6. (a) Energy position of the L4 peak as a function of the c/a ratio, obtained from the experimental and theoretical optical conductivity spectra of ZrSiS, ZrSiSe, ZrGeS, and ZrGeTe, in comparison with the energy difference ΔE between the ungapped band crossings above and below E_F at the X point from Topp *et al.* [7]. Please note the offset of 0.11 eV between the left and the right ordinates. (b) Experimental optical conductivity of ZrSiS for selected external pressures in the high-energy range. The inset: Energy position of the L4 peak in ZrSiS as a function of external pressure. The pressure dependence of the c/a ratio was extracted from Ref. [31].

E_F at X as obtained by Topp *et al.* [7] with the energy of the L4 peak from the experimental and theoretical optical conductivity spectra. Apparently, there is qualitative agreement between the results. The position of the L4 peak in the optical conductivity spectrum may thus serve as a measure for the energy difference between the ungapped band crossings above and below E_F, which are protected by nonsymmorphic symmetry.

The influence of the interlayer bonding on the electronic structure is further corroborated by pressure-dependent optical studies on ZrSiS up to 3.6 GPa. This pressure is below the critical pressure of the structural phase transition observed in Ref. [31]. Generally, applying hydrostatic pressure to a material is a direct and superior way to tune the dimensionality of a material [32,33]. For a layered material, hydrostatic pressure is expected to mostly affect the lattice parameter along the direction with the highest compressibility (at least, for moderate pressures), which is the direction perpendicular to the layers. Hence, under external pressure, the distance between the layers is expected to decrease, leading to an increase in the interlayer bonding. According to the optical conductivity of ZrSiS for selected hydrostatic pressures [see Fig. 6(b)], the L4 peak shifts to higher energy with increasing external pressure. This finding is consistent with the observed chemical pressure effect [34].

V. CONCLUSION

The comparative study of the optical conductivity for the compounds ZrSiY with Y = S, Se, Te and ZrGeY with Y = S, Te revealed a similar optical conductivity profile, namely, a distinct U shape ending at a sharp peak for all studied materials except ZrSiTe. The U shape of the optical conductivity correlates with the nodal-line electronic structure. The low-frequency boundary of the U region correlates with the deviations from a flat nodal line. The sharp peak at the high-frequency limit of the U-shaped region has its origin in the transitions between almost parallel bands in the vicinity of the X and R points of the Brillouin zone. Its energy position may serve as a measure for the energy difference between the ungapped band crossings above and below E_F at the X and R points. The energy position of the peak significantly depends on the interlayer bonding of the system correlated with the c/a ratio, which can be tuned by chemical and external pressures. For ZrSiTe with the largest c/a ratio, the optical conductivity profile is very different due to another pair of crossing bands in the vicinity of E_F, corrugating the nodal-line electronic structure.

ACKNOWLEDGMENTS

C.A.K. acknowledges financial support from the Deutsche Forschungsgemeinschaft (DFG), Germany through Grant No. KU 1432/13-1. This work was supported by the ERC Grant Agreement No. 646807 under EU Horizon 2020 (J.F.A., J.K.). The sample synthesis and characterization efforts were supported by the US Department of Energy under Grant No. DE-SC0019068.

[1] C. Lee, X. Wei, J. W. Kysar, and J. Hone, Science **321**, 385 (2008).

[2] K. I. Bolotin, K. J. Sikes, Z. Jiang, M. Klima, G. Fudenberg, J. Hone, P. Kim, and H. L. Stormer, Solid State Commun. **146**, 351 (2008).

[3] A. A. Balandin, S. Ghosh, W. Bao, I. Calizo, D. Teweldebrhan, F. Miao, and C. N. Lau, Nano Lett. **8**, 902 (2008).

[4] Please note that there are additional surface states in ZrSiS and related compounds according to angle-resolved photoemission studies combined with band-structure calculations [5,6,35]. However, these additional surface states are not relevant for our optical study, which probes the bulk electronic properties.

[5] M. Neupane, I. Belopolski, M. M. Hosen, D. S. Sanchez, R. Sankar, M. Szlawska, S.-Y. Xu, K. Dimitri, N. Dhakal, P. Maldonado, P. M. Oppeneer, D. Kaczorowski, F. Chou, M. Z. Hasan, and T. Durakiewicz, Phys. Rev. B **93**, 201104(R) (2016).

[6] L. M. Schoop, M. N. Ali, C. Strasser, A. Topp, A. Varykhalov, D. Marchenko, V. Duppel, S. S. P. Parkin, B. V. Lotsch, and C. R. Ast, Nat. Commun. **7**, 11696 (2016).

[7] A. Topp, J. M. Lippmann, A. Varykhalov, V. Duppel, B. V. Lotsch, C. R. Ast, and L. M. Schoop, New J. Phys. **18**, 125014 (2016).
[8] Y.-Y. Lv, B.-B. Zhang, X. Li, S.-H. Yao, Y. B. Chen, J. Zhou, S.-T. Zhang, M.-H. Lu, and Y.-F. Chen, Appl. Phys. Lett. **108**, 244101 (2016).
[9] R. Sankar, G. Peramaiyan, I. P. Muthuselvam, C. J. Butler, K. Dimitri, M. Neupane, G. N. Rao, M.-T. Lin, and F. C. Chou, Sci. Rep. **7**, 40603 (2017).
[10] J. Hu, Z. Tang, J. Liu, Y. Zhu, J. Wei, and Z. Q. Mao, Phys. Rev. B **96**, 045127 (2017).
[11] S. Pezzini, M. R. van Delft, L. M. Schoop, B. V. Lotsch, A. Carrington, M. I. Katsnelson, N. E. Hussey, and S. Wiedmann, Nat. Phys. **14**, 178 (2017).
[12] C. Wang and T. Hughbanks, Inorg. Chem. **34**, 5524 (1995).
[13] S. Klemenz, S. Lei, and L. M. Schoop, arXiv:1808.06619.
[14] M. B. Schilling, L. M. Schoop, B. V. Lotsch, M. Dressel, and A. V. Pronin, Phys. Rev. Lett. **119**, 187401 (2017).
[15] T. Habe and M. Koshino, Phys. Rev. B **98**, 125201 (2018).
[16] J. Hu, Z. Tang, J. Liu, X. Liu, Y. Zhu, D. Graf, K. Myhro, S. Tran, C. N. Lau, J. Wei, and Z. Q. Mao, Phys. Rev. Lett. **117**, 016602 (2016).
[17] J. Hu, Y. L. Zhu, D. Graf, Z. J. Tang, J. Y. Liu, and Z. Q. Mao, Phys. Rev. B **95**, 205134 (2017).
[18] D. B. Tanner, Phys. Rev. B **91**, 035123 (2015).
[19] M. I. Eremets and Y. A. Timofeev, Rev. Sci. Instrum. **63**, 3123 (1992).
[20] A. Pashkin, M. Dressel, and C. A. Kuntscher, Phys. Rev. B **74**, 165118 (2006).
[21] P. Blaha, K. Schwarz, G. K. H. Madsen, D. Kvasnicka, and J. Luitz, *WIEN2K, an Augmented Plane Wave+Local Orbitals Program for Calculating Crystal Properties* (Vienna University of Technology, Vienna, 2001).
[22] A. A. Mostofi, J. R. Yates, G. Pizzi, Y.-S. Lee, I. Souza, D. Vanderbilt, and N. Marzari, Comput. Phys. Commun. **185**, 2309 (2014).
[23] J. Kuneš, R. Arita, P. Wissgott, A. Toschi, H. Ikeda, and K. Held, Comput. Phys. Commun. **181**, 1888 (2010).
[24] R. Singha, A. K. Pariari, B. Satpati, and P. Mandal, Proc. Natl. Acad. Sci. USA **114**, 2468 (2017).
[25] J. P. Carbotte, J. Phys.: Condens. Matter **29**, 045301 (2017).
[26] S. P. Mukherjee and J. P. Carbotte, Phys. Rev. B **95**, 214203 (2017).
[27] S. Ahn, E. J. Mele, and H. Min, Phys. Rev. Lett. **119**, 147402 (2017).
[28] See Supplemental Material at http://link.aps.org/supplemental/10.1103/PhysRevB.99.125154 for further information. Note that Fig. S4 denotes the importance of dipole matrix elements for the in-plane and out-of-plane optical conductivity of ZrSiS.
[29] Accordingly, ZrGeS is closest to the ideal nodal-line system since its low-frequency limit of the U-shaped optical conductivity is the lowest among the studied compounds. It is interesting to note that ZrGeS has the lowest c/a ratio among the studied ZrXY materials.
[30] M. M. Hosen, K. Dimitri, I. Belopolski, P. Maldonado, R. Sankar, N. Dhakal, G. Dhakal, T. Cole, P. M. Oppeneer, D. Kaczorowski, F. Chou, M. Z. Hasan, T. Durakiewicz, and M. Neupane, Phys. Rev. B **95**, 161101(R) (2017).
[31] R. Singha, S. Samanta, S. Chatterjee, A. Pariari, D. Majumdar, B. Satpati, L. Wang, A. Singha, and P. Mandal, Phys. Rev. B **97**, 094112 (2018).
[32] T. Nagata, M. Uehara, J. Goto, J. Akimitsu, N. Motoyama, H. Eisaki, S. Uchida, H. Takahashi, T. Nakanishi, and N. Môri, Phys. Rev. Lett. **81**, 1090 (1998).
[33] A. Pashkin, M. Dressel, M. Hanfland, and C. A. Kuntscher, Phys. Rev. B **81**, 125109 (2010).
[34] Please note that according to Ref. [31] the effect of external pressure on the c/a ratio in ZrSiS is much smaller than the corresponding effect of chemical pressure. Therefore, the effect of external pressure on the energy position of the L4 peak occurs on a much smaller energy scale as compared to the chemical pressure effect shown in Fig. 6(a).
[35] A. Topp, R. Queiroz, A. Grneis, L. Müchler, A. W. Rost, A. Varykhalov, D. Marchenko, M. Krivenkov, F. Rodolakis, J. L. McChesney, B. V. Lotsch, L. M. Schoop, and C. R. Ast, Phys. Rev. X **7**, 041073 (2017).